DOI: 10.1021/ma1013786

Macromolecules
ARTICLE

Thermodynamic Properties of Block Copolymer Electrolytes Containing Imidazolium and Lithium Salts

Nisita S. Wanakule,[†] Justin M. Virgili,[†,‡,⊥] Alexander A. Teran,[†,§] Zhen-Gang Wang,*[,∥] and Nitash P. Balsara*[,†,‡,§]

[†]*Department of Chemical Engineering, University of California, Berkeley, California 94720,* [‡]*Materials Sciences Division, Lawrence Berkeley National Laboratory, Berkeley, California 94720,* [§]*Environmental Energy and Technologies Division, Lawrence Berkeley National Laboratory Berkeley, California 94720, and* [∥]*Division of Chemistry and Chemical Engineering, California Institute of Technology, Pasadena, California 91125.* [⊥]*Current affiliation: The Dow Chemical Company.*

Received June 21, 2010; Revised Manuscript Received August 25, 2010

ABSTRACT: We report on the thermal properties, phase behavior, and thermodynamics of a series of polystyrene-*block*-poly(ethylene oxide) copolymers (SEO) mixed with the ionic species Li[$N(SO_2CF_3)_2$] (LiTFSI), imidazolium TFSI (ImTFSI), and an equimolar mixture of LiTFSI and ImTFSI (Mix). Differential scanning calorimetric scans reveal similar thermal behavior of SEO/LiTFSI and SEO/ImTFSI at the same salt concentrations. Phase behavior and thermodynamics were determined using a combination of small-angle X-ray scattering and birefringence. The thermodynamics of our mixtures can be mapped on to the theory of neat block copolymer phase behavior provided the Flory−Huggins interaction parameter, χ, between the blocks is replaced by an effective χ (χ_{eff}) that increases linearly with salt concentration. The phase behavior and the value of m, the slope of the χ_{eff} versus salt concentration data, were similar for SEO/LiTFSI, SEO/ImTFSI, and SEO/Mix blends. The theory developed by Wang [*J. Phys. Chem. B.* **2008**, *41*, 16205] provides a basis for understanding the fundamental underpinnings of the measured value of m. We compare our experimental results with the predictions of this theory with no adjustable parameters.

Introduction

Block copolymers are known to self-assemble into a wide variety of morphologies such as lamellae (LAM), gyroid (GYR), and hexagonally packed cylinders (CYL) with characteristic length scales on the order of 10−100 nm. Charge transport enabled by the presence of continuous domains such as LAM, CYL, and networks can be exploited to obtain structured polymer electrolyte membranes (PEM).[1−18] Typically, when block copolymers are designed for use as a PEM, one block preferentially solvates the ionic species (e.g., salts), enabling ion conduction. Although an ionic species can be incorporated into the backbone of a polymer chain, we focus on polymer electrolytes where ionic species are added to the polymer. A promising PEM for rechargeable lithium metal batteries is poly(ethylene oxide) (PEO), which readily dissolves lithium salts such as Li[$N(SO_2CF_3)_2$] (LiTFSI). The second block, which is nonconductive, can be tuned to optimize other aspects of the PEM such as mechanical strength. As has been the case with previous studies from our group,[15−17,19] we use PEO blocks to dissolve the salts and polystyrene (PS) blocks to obtain the nonconductive microphase.

The effect of salts on the properties of PEO homopolymers has been studied extensively.[20−24] An overview of this body of work can be found in ref 25. We focus on studies of the phase behavior of PEO/salt mixtures. The nature of both the cations and anions affect the properties of PEO/salt mixtures. It has been reported that the solubility of alkali metal salts with $TFSI^-$ as the counterion in PEO (molecular weight of about 4 kg/mol) increases with decreasing ion radius.[26] In this paper we often use the molar ratio of cations to monomers in the ion-solvating polymer chain or block, r, to quantify the salt concentration in our system. In the case of mixed salts, r includes cations from both salts. The values of r at the solubility limit for LiTFSI, NaTFSI, and KTFSI are 0.67, 0.25, and 0.20, respectively. The phase diagrams of PEO/NaTFSI and PEO/LiTFSI, reported in refs 26 and 21, exhibit important differences. Crystalline intermediate compounds are obtained at EO:Na ratios of 7:1 and 3:1 in PEO/NaTFSI with melting points of 50 and 68 °C, respectively, and at EO:Li ratios of 6:1, 3:1 and 2:1 in PEO/LiTFSI with melting points of 46, 85, and 110 °C, respectively. In the case of PEO/LiTFSI, crystallization of PEO is not observed in compositions between $r = 0.08$ and 0.17, resulting in a window that has been referred to as the crystallinity gap. The crystallinity gap is not found in PEO/NaTFSI or PEO/KTFSI, i.e. there is no suppression of PEO crystallization in the presence of NaTFSI or KTFSI. The solubility limit of alkali metal salts is also affected by changes in the anion. For example, changing the salt from LiTFSI to LiSCN changes the solubility limit from $r = 0.67$ to 0.33. In contrast, the values of r at the solubility limit for KSCN and KTFSI are within experimental error (0.20). Changing the anion from $TFSI^-$ to $CF_3SO_2N(CH_2)_3OCH_3^-$ ($MPSA^-$) results in a dramatic change in phase behavior. The phase behavior of PEO/LiMPSA is that of a simple binary eutetic with no intermediate crystalline compounds or crystallinity gaps. In contrast, the phase behavior of PEO/KMPSA contains a large crystallinity gap.

It is evident from the above discussion that the behavior of both crystalline and amorphous PEO/salt mixtures depends on the chemical structure of the anion and the cation. Effects such as ion dissociation, charge delocalization, and dispersive interactions between the ions and the polymer (particularly for large cations) play an important role in determining phase behavior.

*Authors to whom correspondence should be addressed.

 Published on Web 09/13/2010

Some insight into the underpinnings of the observed phase behavior is obtained by measuring the ionic conductivity of PEO/salt mixtures. Studies of LiTFSI, NaTFSI, and KTFSI in PEO show that the conductivity values of these systems in the low salt concentration limit have a weak dependence on the cation (LiTFSI and NaTFSI have conductivity values of 1.1×10^{-3} S/cm while KTFSI has a value of 0.9×10^{-3} S/cm at $r = 0.03$).[26] This is probably because most of the current is carried by the anion. The measured transference number of the cation in LiTFSI/PEO mixtures, the most widely studied system, ranges from 0.17 to 0.6 (for r of 0.03 to 0.20).[27] The nature of the anion has a profound effect on conductivity. The conductivity values of PEO/LiTFSI mixtures at low temperatures is several-fold higher than that of PEO mixed with $LiClO_4$ or $LiCF_3SO_3$ at the same r.[21,22,25,28] This is principally due to the large $TFSI^-$ anion, which has high charge delocalization allowing for greater dissociation.[25] Spectroscopic studies indicate that the dissociation of alkali metal salts in PEO is complicated by the formation of ion pairs, triplets (Li^+ associated with an ion pair), and other complex aggregates.[23]

Another class of TFSI-containing compounds is ionic liquids (IL), such as imidazolium TFSI (ImTFSI) and pyrrolidinium TFSI. Whereas salts are crystalline solids in the temperature range of interest, ILs are liquids at moderate temperatures. These compounds are of great current interest due to their unique physiochemical properties (e.g., nonflammability, negligible vapor pressure, electrochemical stability, etc.) and their ability to promote ion conduction.[29−34] Their liquid structure and high ionic conductivity (at 30 °C, ILs have conductivity values on the order of 10^{-3} to 10^{-2} S/cm[32,35,36]) have been shown to enhance conductivity of PEO/LiTFSI systems. Thus, ionic liquids have been investigated as a supporting electrolyte for the PEO/LiTFSI system for lithium batteries.

The thermal properties of IL-containing PEO systems differ from PEO/LiTFSI systems. DSC thermograms of PEO/LiTFSI/IL systems have distinct crystallinity peaks corresponding to either PEO crystals or $P(EO)_6$LiTFSI crystals at all ionic liquid concentrations.[32,33,37,38] That is, PEO/LiTFSI/IL mixtures do not exhibit full suppression of the crystallinity peak as seen in the crystallinity gap of PEO/LiTFSI systems. There is some suppression of the crystalline phases. Zhu et al.[37] measured the decrease in ΔH_m upon addition of 1-ethyl-3-methylimidazolium TFSI (EMITFSI) or *N*-methyl-*N*-propylpiperidinium TFSI (PP_{13}TFSI) to a sample of $P(EO)_{20}$LiTFSI. In the equimolar IL to LiTFSI case, ΔH_m decreases from 73.94 J/g for PEO/LiTFSI ($r = 0.05$) to 41.66 J/g for PEO/LiTFSI/EMITFSI ($r = 0.10$) and 36.46 J/g for PEO/LiTFSI/PP_{13}TFSI ($r = 0.10$). Similarly, Cheng et al.[38] measured a decrease in ΔH_m for $P(EO)_{20}$LiTFSI systems with 1-butyl-4-methylpyridinium (BMPyTFSI). At $r = 0.10$, equimolar LiTFSI:BMPyTFSI, $\Delta H_m = 20.89$ J/g. Despite the presence of crystals in PEO/LiTFSI/IL systems, room temperature conductivity of these samples are still high. At 20 °C, the conductivity values of PEO/LiTFSI systems with various *N*-butyl-*N*-methylpyrrolidinium range from 2.02×10^{-6} to 1.28×10^{-4} S/cm.[34] In the case of pure EMITFSI in PEO or SEO studied by Simone et al.,[36] complete suppression of crystallinity is seen at $r = 0.20$ and $r = 0.25$. Simone et al. also note a change in SEO phase behavior with increasing EMITFSI content. As EMITFSI concentration is increased, the samples transform from CYL (with minor phase PEO), to LAM, to CYL (with major phase PEO).

In this paper, we study the effect of adding the salt LiTFSI (melting point of 234 °C) and the ionic liquid ImTFSI (melting point of 72 °C) to polystyrene-*block*-poly(ethylene oxide) (SEO) copolymers on thermodynamics and morphology. Figure 1 shows the structure of Li^+, $TFSI^-$, and Im^+. Li^+ is small and spherical, while Im^+ is large and planar. For simplicity, we use the term "salt" to refer to either ImTFSI or LiTFSI. Some of the relevant characteristics of the salts are given in Table 1. One expects effects such as ion dissociation, charge delocalization, and dispersive interactions between the ions and the polymer to affect salt/block copolymer thermodynamics, as was the case with PEO/salt mixtures. The added factor in the system of interest is the dispersive interaction between polystyrene (PS) and PEO blocks in the SEO copolymer. The phase behavior of neat block copolymers are governed by the volume fraction of one of the blocks, ϕ (we use the PEO block volume fraction in this paper), the degree of polymerization, N, and the Flory−Huggins interaction parameter, χ, which is a measure of the dispersive interactions between the two monomers comprising the block copolymer.[39] Previous experimental[17,18,40] and theoretical[41] studies have demonstrated that the effect of added salt results in an increase of the "effective" Flory−Huggins interaction parameter, χ_{eff}. In other words, the framework developed for describing the thermodynamics of neat block copolymers can be used to describe the thermodynamics of block copolymer/salt mixtures provided χ is replaced by χ_{eff}. Similar concepts were used to describe the thermodynamic properties of block copolymer solutions.[42−45] Since the added salt resides primarily in one of the phases, the concomitant changes in ϕ must be taken into account. In addition, a simple linear relationship between χ_{eff} and r has been proposed:

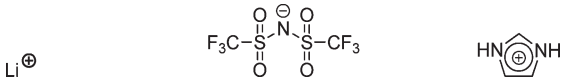

Figure 1. Schematic of Li^+ cation, $TFSI^-$ anion, and Im^+ cation.

Table 1. Properties of LiTFSI and ImTFSI ions

salt	melting point (°C)	cation radius (nm)	anion radius (nm)
LiTFSI	234	0.076	0.381
ImTFSI	72	0.210	0.381

$$\chi_{eff} = \chi_{neat} + mr \quad (1)$$

Here, χ_{neat} is the Flory−Huggins interaction parameter of the neat copolymer, and m is a system-dependent constant. The effect of salt addition on block copolymer thermodynamics is quantified by the magnitude of m. In the case of LiCl added to polystyrene-*block*-poly(methyl methacrylate) (SMMA) copolymers, χ_{eff} increases from 0.0360 to 0.0368, when r increases from 0 to 0.1, indicating that m is about 10^{-4}.[40] Young et al. found that values of m in the cases of $LiAsF_6$, $LiClO_4$ and $LiCF_3SO_3$ in SEO copolymers are 5.70, 5.53 and 3.90, respectively.[18] Young et al. noted that the effective repulsion between the blocks gets weaker as the Lewis basicity of the anion decreases. In our previous publication, Wanakule et al. reported that m for SEO/LiTFSI is 1.56.[17] The data obtained in ref 17 are consistent with the arguments of Young et al. There is considerable uncertainty in the determination of salt concentration in the SMMA/LiCl mixtures as it was obtained by spectroscopy owing to the immiscibility of the salt in the polymer.[40] No such difficulty arises in the case of mixtures of SEO and lithium salts and the salt concentration can readily be determined gravimetrically. The effect of this on the 4 orders of magnitude difference in the measured values of m in SMMA and SEO is unclear.

Theoretical work by Wang[41] indicates that m can be calculated using independently determined parameters such as the dielectric constants of the two phases, the size of the ions, the extent of dissociation, the dielectric constant of the block copolymer microphases, and the statistical segment lengths of the copolymer chains. In this paper, we compare our experimental data and that reported in ref 18 with the predictions

Table 2. Characterization of copolymers used in this study

polymer	$M_{n,PS}$ (kg/mol)	$M_{n,PEO}$ (kg/mol)	φ(PEO block)	PDI
SEO(5.3−3.0)	5.3	3.0	0.34	1.02
SEO(5.3−3.6)	5.3	3.6	0.38	1.02
SEO(4.6−3.7)	4.6	3.7	0.43	1.02
SEO(6.4−7.2)	6.4	7.2	0.52	1.02
SEO(3.1−5.1)	3.1	5.1	0.60	1.02
SEO(2.3−4.6)	2.3	4.6	0.65	1.02

of the theory developed in ref 41 without resorting to any adjustable parameters.

Experimental Section

Materials. The polystyrene-*block*-poly(ethylene oxide) copolymers used in this study were synthesized by sequential living polymerization using the methods described in refs 46−48. The polystyrene block was synthesized first using *sec*-butyl lithium as the initiator. This was followed by the polymerization of ethylene oxide with P4 *tert*-butylphosphazene base as a catalyst and then terminated with 2-propanol. The copolymers were purified by filtration of the SEO dissolved in benzene through a 0.2 μm filter followed by precipitation in a cold hexane solution. The filtration/precipitation steps were repeated two more times. The molecular weight of the polystyrene block and the polydispersity indices (PDI) of the polystyrene block and overall polymer were obtained by size exclusion chromatography using a Waters 717 plus autosampler instrument equipped with a Waters 486 tunable absorbance detector and Wyatt Tech DAWN EOS light-scattering detector calibrated with polystyrene standards. ^{1}H NMR spectroscopy was used to determine the volume fraction of each block. The polymers used in this study, which we call SEO(xx−yy) where xx and yy are the molecular weights of the PS and PEO blocks in kg/mol respectively, are listed in Table 2.

LiTFSI salt, purchased from Sigma-Aldrich, was heated at 100 °C under vacuum for 1−2 days to get rid of residual moisture and then stored in the glovebox. Imidazole (≥95%) and bis(trifluoromethane)sulfonimide (HTFSI, ≥95%) were purchased from Sigma-Aldrich and purified by sublimation under vacuum. Differential scanning calorimetry (DSC) and ^{1}H NMR were used to assess the purity of the two starting materials. Purified imidazole and HTFSI were combined in equimolar quantities in a glovebox, sealed, and heated in an oven outside the glovebox to 100 °C for 2−3 h to prepare the ionic liquid ImTFSI. The composition of the ionic liquid was confirmed by comparing the measured melting point of the compound, using DSC, with literature.[49]

The copolymers were doped with the salt LiTFSI, the ionic liquid ImTFSI, or a 50:50 molar mixture of the salt and the ionic liquid (Mix). To prepare the doped copolymers, the SEO was first dried at 90 °C under vacuum for 1 day, then immediately brought into the glovebox. A predetermined amount of LiTFSI and/or ImTFSI was added to the polymer. The salt and ionic liquid concentration in our copolymers is quantified by the molar ratio of cation to ethylene oxide moieties, r, which ranges from 0.01 to 0.125. Samples were typically freeze-dried, and then annealed in a sample cell at 110 °C for 2 days. Ionic liquid samples were prepared by solvent casting from dry dichloromethane, and annealed at 110 °C inside a glovebox for about 12 h.

Structural Characterization. The structure of the polymer electrolyte was determined by small-angle X-ray scattering (SAXS). SAXS samples were sealed off in a custom-designed-airtight sample holder with Kapton windows and annealed for 1−3 days at 100 °C. Because of the hygroscopic nature of the salts, glovebox integrity was maintained throughout all stages of experimentation.

Measurements were performed at beamline 7.3.3 at the Advanced Light Source (ALS) at Lawrence Berkeley National Laboratory and beamline 1−4 at the Stanford Synchrotron Radiation Laboratory (SSRL). Samples were mounted on a custom-built temperature stage and annealed at each temperature for 20 min before taking measurements. Longer annealing times were not practical due to limited access to the instrumentation. A silver behenate sample was used as a standard. Full two-dimensional scattering patterns were collected on an ADSC CCD detector. The scattering patterns from ALS were reduced using the Nika program for Igor Pro available from Jan Ilavsky at Argonne National Laboratory, and data from SSRL were reduced using a program written by John Pople at SSRL.

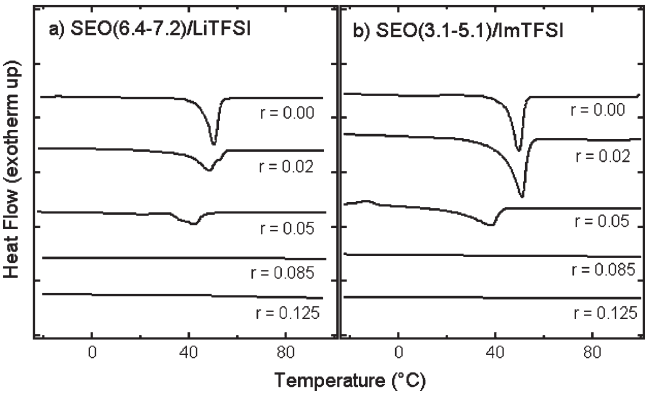

Figure 2. DSC scans of SEO with LiTFSI and ImTFSI.

Order-to-disorder transition (ODT) temperatures were confirmed using birefringence. Birefringence measurements were performed using the setup described in ref 50 with a plane-polarized laser beam with wavelength 633 nm as the source. The samples were subjected to two heating and cooling cycles with temperature steps of approximately 10 °C. Minimum annealing times for the heating and cooling runs at each temperature were 20 and 45 min, respectively. The intensity of the beam after it passed through the sample placed between two crossed polarizers was recorded with a photodiode as a function of temperature and then normalized by the incident intensity.

Differential scanning calorimetry (DSC) was performed on a TA Instruments DSC 2920. The samples were crimped in a glovebox using hermetically sealed pans and placed inside a container with desiccant for transfer to the DSC. Indium and dodecane were used as calibration standards for the DSC. Samples underwent three heating and cooling cycles.

Results and Discussion

We first focus on the thermal properties of SEO with LiTFSI and ImTFSI. Parts a and b of Figure 2 show DSC scans of SEO(6.4−7.2) with varying concentrations of LiTFSI and SEO-(3.1−5.1) with varying levels of ImTFSI, respectively, at 5 °C/min. The melting point of the PEO/salt microphase and the enthalpy of melting, ΔH_m, decrease with increasing r in both SEO/LiTFSI and SEO/ImTFSI. The melting peak temperature decreases from 50 to 40 °C as r is increased from 0 to 0.05, while ΔH_m values decrease from 55 to 19 J/g in SEO(6.4−7.2)/LiTFSI and from 63 to 32 J/g in SEO(3.1−5.1)/ImTFSI. At r values higher than 0.05, we observe complete suppression of crystallinity. This behavior is consistent with observations of Lascaud et al. on PEO/LiTFSI homopolymer/salt mixtures.[21] They measured a decrease in melting temperatures with increasing salt concentration up to $r = 0.08$. Between $r = 0.08$ and 0.17, a crystallinity gap appears in the PEO/LiTFSI phase diagram. The fact that the phase behavior of SEO/LiTFSI and SEO/ImTFSI data agrees with PEO/LiTFSI data indicates that the salts are preferentially segregating to the PEO-rich domains. This is due to the higher dielectric constant, ε, of the PEO domain (estimates of ε_{PEO} range from 4 to 8,[51−54] while that of ε_{PS} ranges from 2 to 4[55,56]), and specific interactions between ether oxygens and Li^+.[19,36]

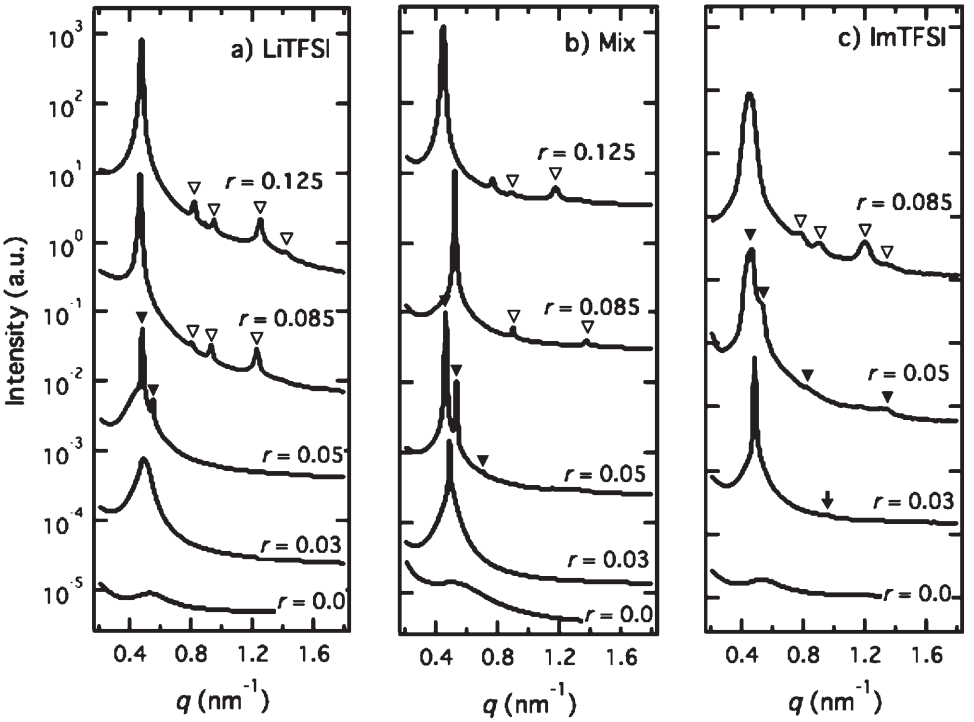

Figure 3. SAXS profiles for SEO(3.1−5.1) with varying concentrations of (a) LiTFSI, (b) Mix, and (c) ImTFSI at 100 °C. Arrows, closed upside down triangles and open upside down triangles indicate higher order reflections of LAM, GYR, and CYL, respectively.

One can also view salts as highly selective solvents. Extensive studies by Lodge et al.[57,58] have shown that this leads to stabilization of the ordered phase. This behavior is apparent in the SAXS profiles of SEO(3.1 − 5.1) at 100 °C with varying concentrations of LiTFSI, a 50:50 molar mixture of both LiTFSI and ImTFSI (Mix), and ImTFSI as shown in Figure 3. Although the neat polymer is disordered (DIS) at all temperatures, changing r allows us to access a wide variety of morphologies including lamellar (LAM), gyroid (GYR) and hexagonally packed cylinders (CYL). At an r value of 0.03, the primary peaks in the SEO(3.1 − 5.1) with ImTFSI and Mix are significantly sharper than those at $r = 0$ (full-width-at-half maximum of peak decreases by an order of magnitude). Higher order peaks can be seen at $2q^*$ for SEO(3.1 − 5.1)/ImTFSI, shown by the arrow in Figure 3b, indicating that the samples are LAM. Following the arguments presented in ref 17, we conclude that the addition of salt leads to a DIS to LAM transition in these samples at 100 °C. SEO(3.1 − 5.1)/Mix samples contain the higher order $2q^*$ peaks at lower temperatures, but not in the vicinity of the ODT at 100 °C. The loss of higher order peaks is often observed in weakly ordered block copolymers due to effects in the vicinity of the ODT such as limited long-range order and diminished contrast between the coexisting phases. At $r = 0.05$, SEO(3.1−5.1)/LiTFSI and SEO(3.1 − 5.1)/Mix samples are clearly GYR, with prominent peaks at $\sqrt{(4/3)}q^*$ and $\sqrt{(7/3)}q^*$ (for the Mix case), as indicated by the upside-down filled triangles in Figure 3a and b. For the sample with ImTFSI at $r = 0.05$ (Figure 3c), a shoulder is apparent at $\sqrt{(4/3)}q^*$.[59] Higher order reflections at $\sqrt{(10/3)}q^*$ and $\sqrt{(24/3)}q^*$ further confirm the GYR structure in this sample. At $r = 0.085$ and above for SEO(3.1−5.1) combined with LiTFSI, Mix, and ImTFSI, the samples are clearly CYL with higher order peaks at $\sqrt{3}q^*$, $\sqrt{4}q^*$, $\sqrt{7}q^*$, and $\sqrt{9}q^*$.

Similar experiments were carried out over a range of temperatures between 70 and 150 °C, and a phase diagram (Figure 4) was constructed using SAXS profiles of SEO(3.1−5.1) with LiTFSI and ImTFSI at $r = 0$, 0.02, 0.03, 0.05, 0.085, and 0.125. Note that we generalize the definition of r to be the ratio

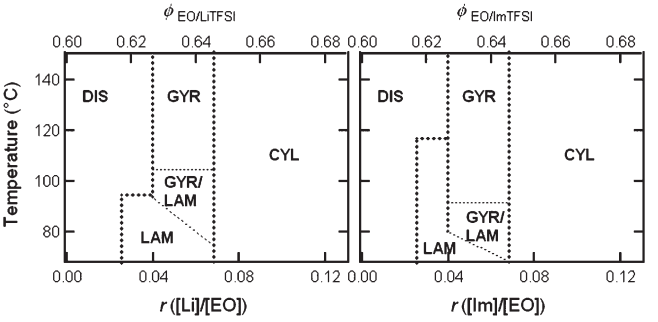

Figure 4. Phase behavior of SEO(3.1−5.1) at various temperatures and concentrations of (a) LiTFSI and (b) ImTFSI, where DIS is the disordered phase, GYR is the gyroid phase, LAM is the lamellar phase, CYL is the hexagonally packed cylinders phase, and GYR/LAM is coexistence of GYR and LAM. Dashed lines are locations of transitions within ±5 °C. The error in r is ±0.005 at the DIS/LAM transition, ±0.01 at the DIS/GYR transition, and ±0.0175 at the GYR/CYL transition.

of all cations to EO monomers in the mixtures. The top axes of Figure 4 show is the calculated volume fraction of the PEO-rich phase, $\phi_{EO/Salt}$, in the presence (or absence) of salt. The changes in $\phi_{EO/Salt}$ due to changes in r were calculated using the relationship between the density of PEO/LiTFSI phase and salt concentration, as described in ref 27. Similar density data were not available for PEO/ImTFSI mixtures. We have assumed that the dependence of $\phi_{EO/Salt}$ on r for PEO/ImTFSI and PEO/LiTFSI are identical. The series of phase transitions shown in Figure 4 are the result of changes in both χ_{eff} and $\phi_{EO/Salt}$ with increasing r.

The neat polymer is disordered (DIS) at all temperatures. At temperatures below 90 °C, we find that as the salt concentration is increased from $r = 0.02$ to $r = 0.03$, the LAM phase is favored over the DIS phase, indicating a disorder-to-order transition (DOT) at $r = 0.025 \pm 0.005$ for SEO(3.1−5.1) with LiTFSI or ImTFSI. The LAM phase persists at $r = 0.03$ up to $T = 93$ °C for LiTFSI/SEO(3.1−5.1) and $T = 117$ °C for ImTFSI/SEO(3.1−5.1).

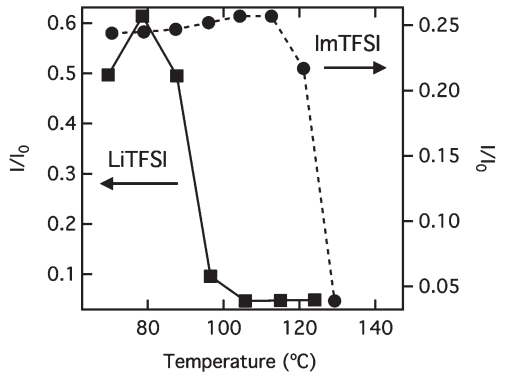

Figure 5. Birefringence detection of the ODT temperatures for SEO-(3.1−5.1) at $r = 0.03$ for LiTFSI (■) and ImTFSI (●).

Locations of ODTs and OOTs were confirmed with birefringence, as described in ref 17, with a precision of ±5 °C. Figure 5 plots the birefringence signal (I/I_0), where I is the measured intensity and I_0 is the incident intensity, as a function of temperature for SEO-(3.1−5.1) at $r = 0.03$ for samples with LiTFSI and ImTFSI. The ODT temperatures are at 93 °C for SEO(3.1−5.1)/LiTFSI and at 117 °C for SEO(3.1−5.1)/ImTFSI.

Above these respective ODTs, Figure 4 shows a DIS to GYR or GYR/LAM coexistence at $r = 0.04 \pm 0.01$ instead of a DIS to LAM transition. For GYR/LAM coexistence, higher order reflections for both systems are seen in the SAXS profiles, and the birefringence signals decreased gradually with temperature instead of a step decrease in intensity which typically occurs at transitions, as described in ref 17. At $r = 0.068 \pm 0.018$ and higher (up to $r = 0.125$), CYL is obtained, regardless of temperature. We note in passing that the Gibbs phase rule requires coexisting phases to exist at each boundary between single-phase regions. The phase rule also requires the presence of a thin pure GYR phase between the coexistence region and the CYL phase. The fact that these features are not observed simply implies that the windows are narrower than the width of steps used to determine the phase diagram.

In general, SEO/LiTFSI and SEO/ImTFSI show similar phase behavior. Minor differences occur around $r = 0.03$, where the ImTFSI stabilizes the LAM phase to a higher temperature than LiTFSI (Figure 4 and Figure 5). This suggests that the cation plays a minor role in determining the phase behavior of SEO/salt mixtures. There has been considerable focus on the liquid-like structure of EO monomers solvating the Li^+ ion due to a match in the spacing between the ether oxygens in the PEO chains and the radius of the solvation shell.[60−63] It is likely that the solvation shell around the Im^+ ion is very different from that of the Li^+ ion due to the differences in ion radius and shape. The fact that these differences have little effect on the phase behavior of SEO/salt mixtures is somewhat surprising. This result cannot be anticipated from the strong effect of cation size on the properties of salt/PEO mixtures as discussed in the Introduction.

If we picture the well-known block copolymer phase diagram,[64−68] the effect of adding salt to the SEO copolymer corresponds to a "movement" from a point on the phase diagram in the disordered state near the middle of the phase diagram diagonally up and to the right, toward higher values of χ_{eff} and $\phi_{EO/Salt}$. The observed movement in block copolymer/salt mixtures is similar to that obtained in block copolymer/selective solvent mixtures.[69]

We can quantify the increase in χ_{eff} as a function of r by exploiting well-known relationships between χ and the ODT. By studying the phase behavior of several other SEO/salt mixtures in a similar manner to the analysis of SEO(3.1 − 5.1) above, ODTs at various salt concentrations were obtained. The results in these systems are summarized in Table 3. Included in this list are binary mixtures of SEOs with LiTFSI, ImTFSI, and ternary mixtures of SEOs with 50:50 (mole basis) mixtures of LiTFSI:ImTFSI (labeled as Mix in Table 3). In the case of the Mix, r includes cations of both salts. The phase behavior reported in Table 3 was obtained using a combination of SAXS and birefringence. In the case of SEO(4.6−3.7) doped with ImTFSI, we conclude that ODT occurs at $r = 0.015 \pm 0.005$ since it is DIS at $r = 0.01$ and CYL at $r = 0.02$ across the accessible temperature window.

Table 3. List of Polymer Systems and Locations of Order−Disorder Transition Temperatures[a]

polymer	salt	r	ODT (°C)
SEO(6.4−7.2)	N/A	0	95
SEO(5.3−3.6)	LiTFSI	0.019	95
SEO(4.6−3.7)	LiTFSI	0.02	115
SEO(5.3−3.0)	LiTFSI	0.027	105
SEO(3.1−5.1)	LiTFSI	0.03	93
SEO(2.3−4.6)	LiTFSI	0.05	130
SEO(4.6−3.7)	ImTFSI	0.01	DIS
SEO(4.6−3.7)	ImTFSI	0.02	CYL
SEO(3.1−5.1)	ImTFSI	0.03	117
SEO(3.1−5.1)	Mix	0.03	80
SEO(2.3−4.6)	Mix	0.05	130

[a] In cases where no ODT is observed between 50 to 150 °C, the structure is given instead.

Table 4. List of Parameters Used in Equations 2 and 3 To Determine χ_{eff} from Experimental Results

polymer	r	N	$\phi_{EO/Salt}$	S_1	S_2
SEO(6.4−7.2)	0	219	0.52	10.6	17.5
SEO(5.3−3.6)	0.019	145	0.395	11.3	19.7
SEO(4.6−3.7)	0.01	135	0.436	10.7	18.9
SEO(4.6−3.7)	0.02	135	0.443	10.7	18.8
SEO(5.3−3.0)	0.027	136	0.357	12.4	21.8
SEO(3.1−5.1)	0.03	131	0.62	11.8	20.8
SEO(2.3−4.6)	0.05	110	0.68	13.9	25.3

In our previous publication,[17] we employed Leibler's mean field theory on the thermodynamics of block copolymer melts to determine χ_{eff} of the SEO/LiTFSI mixtures. According to Leibler:[39]

$$(\chi_{eff} N)_{ODT} = S_1(\phi_{EO/Salt}) \quad (2)$$

where N is defined by $N = (v_S/v_0)N_{PS} + (v_{EO}/v_0)N_{PEO}$, using $v_0 = 0.1$ nm^3, v_{EO} is the volume of the PEO monomer (0.069 nm^3), v_S is the volume of the PS monomer (0.179 nm^3), N_{PS} is the number of styrene monomers in the PS block, N_{PEO} is the number of EO monomers in the PEO block, and $S_1(\phi_{EO/Salt})$ is a variable that depends solely on the volume fraction of the EO-rich microphase. The values of $\phi_{EO/Salt}$ and N corresponding to each system are given in Table 4.

Using eq 2 and Tables 3 and 4, the $\chi_{eff,\ MeanField}$ for each polymer/salt combination is calculated. Figure 6 plots $\chi_{eff,\ MeanField}$ vs r for SEO/LiTFSI mixtures (closed squares), SEO/Mix (closed triangles), and SEO/ImTFSI mixtures (closed circles). We note that SEO(2.3−4.6)/ImTFSI at $r = 0.05$ (the highest ImTFSI concentration probed for this particular polymer) was macrophase separated (salt precipitation was visible to the naked eye). All of the other samples remain transparent over the temperature range of the experiments. This indicates that the solubility of ImTFSI in SEO(2.3−4.6) is less than that of LiTFSI. The line through the points in Figure 6 is the linear least-squares fit through all the mean-field data with the corresponding fit equation, $\chi_{eff,\ MeanField}$ as a linear function of r indicated in the figure. This linear relationship corresponds with eq 1 with the slope of the line, m, equal to 1.52 ± 0.2. The fact that the data for all salt/SEO mixtures lie on the same line indicates that despite the numerous differences between LiTFSI and ImTFSI including

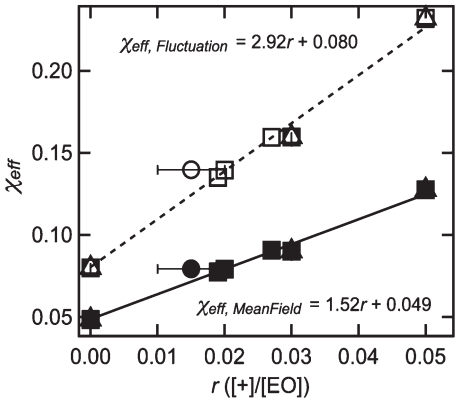

Figure 6. Plot of χ_{eff} vs r for LiTFSI (squares), ImTFSI (circles), and 50:50 Mix of both (triangles) in SEO from the mean-field calculated χ_{eff} using eq 2 (closed markers) and fluctuation corrected χ_{eff} using eq 3 (open markers).

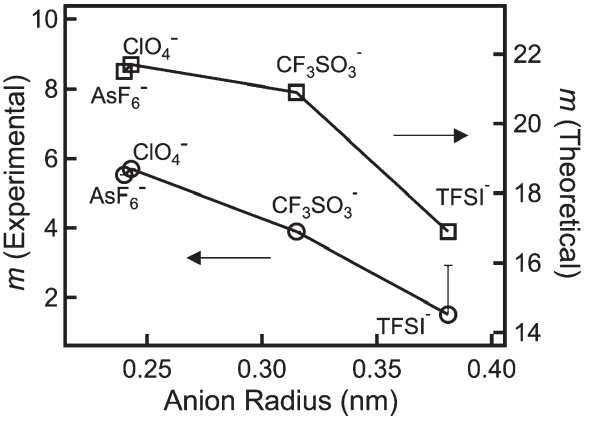

Figure 7. Comparison of theoretical (□) and experimental (○) m values for various anions. Anion size obtained from refs 72−74**.** Theoretical values of m were calculated using eq 5 and experimental values of m for $CF_3SO_3^-$, ClO_4^-, and AsF_6^- obtained from ref 18. The $TFSI^-$ value is from the mean-field calculations (eq 2) with an error bar to indicate the fluctuation-corrected value (eq 3).

cation size and physical state, the thermodynamics of these SEO/salt systems is dominated by the interactions between the $TFSI^-$ anion and PEO. This is in sharp contrast to the phase behavior of PEO/salt mixtures, which depends on the chemical structure of both the cation and the anion.

We also use the more elaborate theory of Fredrickson and Helfand that includes the effect of composition fluctuations on the thermodynamics of block copolymers. In this theory, $(\chi_{eff}N)_{ODT}$ depends on both $\phi_{EO/Salt}$ and N:[65]

$$(\chi_{eff}N)_{ODT} = S_2(N, \phi_{EO/Salt}) \quad (3)$$

For a symmetric block copolymer, Fredrickson and Helfand predict the location of the ODT to occur at $(\chi N)_{ODT} = 10.495 + 41.022N^{-1/3}$, which is equivalent to S_2 at $\phi_{EO/Salt} = 0.5$. As a first approximation, we have calculated values of S_2 at other $\phi_{EO/Salt}$ using

$$S_2(N, \phi_{EO/Salt}) = \alpha(N)S_1(\phi_{EO/Salt}) \quad (4)$$

where $\alpha(N) = 1 + 3.91N^{-1/3}$ is the ratio S_2/S_1 at $\phi_{EO/Salt} = 0.5$. In the small chain length limit ($N = 10^4$), the fluctuation corrected phase boundary is approximately parallel to the mean field calculated curve from $\phi = 0.3$ to 0.7. Since fluctuation effects are important in low molecular weight systems, one expects significant corrections to the mean-field calculations. Figure 6 also shows the relationship between $\chi_{eff,\,Fluctuation}$ and r calculated using eq 3 for SEO/LiTFSI, SEO/ImTFSI, and SEO/Mix. The values of m and χ_{neat} using the fluctuation corrected calculation are about a factor of 2 higher than those of the mean-field calculation (2.92 ± 0.4 and 0.080 instead of 1.52 ± 0.2 and 0.049, respectively). The literature value of χ_{neat} for SEO is 0.048 at 100 °C.[70,71] This value, which was determined using the random phase approximation, is in agreement with our mean-field analysis for neat SEO. Our analysis ignores the temperature-dependence of χ_{eff}, which appears to be much weaker than the m-dependence of χ_{eff}.

In ref 18, Young et al experimentally measured m for mixtures of SEO with $LiCF_3SO_3$, $LiClO_4$, and $LiAsF_6$. In that paper, they used SEO copolymers with molecular weights that were significantly higher than those used in this paper. They compared the observed increase in the domain spacing with added salt and used the strong segregation theory of neat block copolymers to infer the effect of salt on χ_{eff} and m. Their values of χ_{eff} were determined relative to the value of χ_{neat} obtained from literature.[68] The experimental values of m for $TFSI^-$, $CF_3SO_3^-$, ClO_4^-, and AsF_6^- as a function of anion radius are plotted in Figure 7.

The m value for $TFSI^-$ using mean-field calculations is plotted with an error bar, the edge of which indicates the fluctuation-corrected value.

An expression for m in the mean field limit is derived in ref 41 by combining Flory-Huggins theory with the Born energy for solvating ions and the translational entropy of the ions. In that theory, the change in χ arises from several competing effects: the tendency for free, mobile ions to be preferentially solvated by the phase rich in the component of the higher dielectric constant, the translational entropy of the ions, and the local enrichment of the higher dielectric component around an ion in the homogeneous mixture. The Li^+ ions are expected to be tightly bound to the oxygen groups of the EO blocks in both the disordered and ordered states. Thus, their energetics are, to a first approximation, unaffected by microphase separation. By the considerations in ref 41, only the free anions contribute to changing the miscibility of the S and EO blocks. Taking the anions as the dominant contributor and accounting for differences in parameter definitions, we arrive at the following theoretical prediction for m:

$$m_{theory} = \frac{\Delta\chi}{r} = \left(\frac{v_o\varphi_{EO}}{8v_{EO}}\right)\left(\frac{l_o}{a\varepsilon}\right)\left(\frac{l_o}{a\varepsilon} - 4 - \frac{18\lambda_p l_o}{\pi^3\varepsilon a^2}\right)\left(\frac{\Delta\varepsilon}{\varepsilon}\right)^2 \quad (5)$$

where v_o is the reference volume and v_{EO} is the volume of an EO monomer as defined in eq 2, ϕ_{EO} is the volume fraction of PEO in the diblock, l_0 is the Bjerrum length in vacuum (43.6 nm at 110 °C), a is the radius of the anion, λ_p, the packing length (0.287 for a symmetric SEO system) which is defined by v_o/b_{ave}^2 (where b_{ave} is the average statistical segment length defined by $b_{PEO}b_{PS}/(\phi_{EO}b_{PEO} + \phi_S b_{PS})$ and b_{PEO} and b_{PS} are the statistical segment lengths of PEO and PS, respectively, based on a monomer of volume v_o), ε is the average dielectric constant of the polymer defined as $\varepsilon = (\phi_{EO})\varepsilon_{PEO} + (\phi_S)\varepsilon_{PS}$ and $\Delta\varepsilon$ is the difference in dielectric constants defined as $\Delta\varepsilon = \varepsilon_{PEO} - \varepsilon_{PS}$. Details of the derivation of eq 5 are provided in ref 41. For our calculations, we use $\phi_{EO} = 0.5$, $\varepsilon_{PEO} = 7.5$, and $\varepsilon_{PS} = 2.6$. Strictly speaking, the expression derived in ref 41 applies to binary polymer blends. Unpublished calculations show that if the local enrichment effect is neglected, the change in χ is the same for the diblock copolymer and the binary blend. Here we assume that the local enrichment effect is also the same for the diblock copolymer and the binary blend.

Equation 5 is derived assuming that (1) all of the salt ions are dissociated but only the anions contribute to m_{theory}, (2) triplets

and other charged aggregates are not present, and (3) the Li^+ ions are bound to the PEO-blocks in both the ordered and disordered phases while the anions are free. However, charge neutrality and the higher dielectric constant of PEO will bias the anions to PEO-rich locations in both ordered and disordered states. In ref 17, Wanakule et al. measured the conductivity of a variety of SEO/LiTFSI mixtures across the ODT. There was neither a discontinuity at the ODT nor a change in slope in the temperature dependence of the conductivity in the ordered and disordered state. In other words, the temperature dependence of SEO/LiTFSI mixtures obtained from fully ordered systems, fully disordered systems, and systems with accessible ODTs were identical. We take this observation as evidence that the ions in the system have the same PEO-rich local environment regardless of the state of order of the samples. This provides justification for assumption 3 in the analysis.

In Figure 6, we compare the experimental measurements of m as a function of anion size with theoretical predictions, m_{theory}. The only parameter that was varied in the theoretical calculations was the anion radius. We use values of 0.381, 0.315, 0.24, and 0.243 nm as the radii of $TFSI^-$, $CF_3SO_3^-$, ClO_4^-, and AsF_6^-, respectively.[72−74] It is clear that the theory captures the trend seen in the experimental data. However, the theoretically predicted values of m_{theory} are considerably larger than the experimentally determined values of m. For completeness, we note that m_{theory} values calculated assuming that the cations dominate thermodynamics are −245 for Li^+ (a = 0.076 nm) and 26.1 for Im^+ (a = 0.21 nm).

Considering that the values of m_{theory} were calculated using all nonadjustable parameters, the discrepancy between theory and experiment is reasonable. However, there are many possible reasons for the fact that theoretically calculated values of m are larger than experimental measurements. For example, there is a wide range of ε_{PEO} and ε_{PS} reported in literature.[51−56] None of these values were reported for the temperature range of our experiments. We chose ε_{PEO} measured for an amorphous PEO and the median value for ε_{PS}. If, instead, we use values at the extremes of the reported ranges (ε_{PEO} = 4 and ε_{PS} = 3), the calculated values of m_{theory} decreases by a factor of 4. Furthermore, the theory does not account for the formation of charged aggregates and ion pairs directly. Both of these will reduce the ion concentration and increase the effective ion radius, resulting in a reduced m_{theory}. It has also been shown that the addition of lithium salts to PEO increases the dielectric constant of the PEO/salt system. If we use a value of ε_{PEO} = 12 (the dielectric constant measured for a PEO/$LiClO_4$ mixture),[54] the calculated value of m_{theory} also decreases. While many improvements can be proposed, ref 41 provides a starting point for exploring the underpinnings of the phase behavior of block copolymer/salt mixtures.

Conclusions

The thermodynamics and phase behavior of mixtures of SEO copolymers with added salts (LiTFSI, ImTFSI, and mixtures thereof) were studied by SAXS and birefringence. This enables a study of the effect of the cation size and shape on the properties of block copolymer electrolytes. All of our observations were consistent with the assumption that the salts reside exclusively in the PEO-rich microphase. The morphologies obtained as a function of added salt were in agreement with the calculated changes in volume of the PEO-rich microphase due to the presence of salt. In addition to changes in effective composition of the copolymer, the addition of salt increases the effective Flory−Huggins interaction parameter, χ_{eff}, between the PEO/salt system and PS. Surprisingly, the data obtained from mixtures containing LiTFSI and ImTFSI were similar, indicating that the thermodynamics are dominated by the nature of the anion. The parameter m that captures the increase in χ_{eff} with increasing salt concentration, r, obtained from experiments described here and those reported by Young et al.[18] was compared with theoretical predictions of Wang[41] with no adjustable parameters. The qualitative trends seen in the experiments are captured by theory but the predicted values of m are consistently higher than those measured experimentally. It is clear, however, that m decreases with increasing anion size and is independent of the cation size.

Acknowledgment. This work was supported by the National Science Foundation (DMR-0966662, CBET-0965812, and CBET-0966632) and the Batteries for Advanced Transportation Technologies (BATT) Program, supported by the U.S. Department of Energy FreedomCAR and Vehicle Technologies Program. N.S.W. was supported by a National Science Foundation Graduate Research Fellowship. The Advanced Light Source is supported by the Director, Office of Science, Office of Basic Energy Sciences, of the U.S. Department of Energy, under Contract No. DE-AC02-05CH11231. Portions of this research were carried out at the Stanford Synchrotron Radiation Lightsource, a national user facility operated by Stanford University on behalf of the U.S. Department of Energy, Office of Basic Energy Sciences. We thank Shrayesh Patel for helpful discussions and Ariel Tsui for experimental help.

References and Notes

(1) Soo, P. P.; Huang, B. Y.; Jang, Y. I.; Chiang, Y. M.; Sadoway, D. R.; Mayes, A. M. *J. Electrochem. Soc.* **1999**, *146* (1), 32–37.
(2) Ruzette, A. V. G.; Soo, P. P.; Sadoway, D. R.; Mayes, A. M. *J. Electrochem. Soc.* **2001**, *148* (6), A537–A543.
(3) Wright, P. V. *MRS Bull.* **2002**, *27* (8), 597–602.
(4) Trapa, P. E.; Huang, B. Y.; Won, Y. Y.; Sadoway, D. R.; Mayes, A. M. *Electrochem. Solid State Lett.* **2002**, *5* (5), A85–A88.
(5) Cho, B. K.; Jain, A.; Gruner, S. M.; Wiesner, U. *Science* **2004**, *305* (5690), 1598–1601.
(6) Deluca, N. W.; Elabd, Y. A. *J. Polym. Sci., Part B: Polym. Phys.* **2006**, *44* (16), 2201–2225.
(7) Sadoway, D. R.; Huang, B. Y.; Trapa, P. E.; Soo, P. P.; Bannerjee, P.; Mayes, A. M. *J. Power Sources* **2001**, *97−8*, 621–623.
(8) Sadoway, D. R. *J. Power Sources* **2004**, *129* (1), 1–3.
(9) Mui, S. C.; Trapa, P. E.; Huang, B.; Soo, P. P.; Lozow, M. I.; Wang, T. C.; Cohen, R. E.; Mansour, A. N.; Mukerjee, S.; Mayes, A. M.; Sadoway, D. R. *J. Electrochem. Soc.* **2002**, *149* (12), A1610–A1615.
(10) Niitani, T.; Shimada, M.; Kawamura, K.; Kanamura, K. *J. Power Sources* **2005**, *146* (1−2), 386–390.
(11) Niitani, T.; Shimada, M.; Kawamura, K.; Dokko, K.; Rho, Y. H.; Kanamura, K. *Electrochem. Solid State Lett.* **2005**, *8* (8), A385–A388.
(12) Ryu, S. W.; Trapa, P. E.; Olugebefola, S. C.; Gonzalez-Leon, J. A.; Sadoway, D. R.; Mayes, A. M. *J. Electrochem. Soc.* **2005**, *152* (1), A158–A163.
(13) Bullock, S. E.; Kofinas, P. *J. Power Sources* **2004**, *132* (1−2), 256–260.
(14) Gopinadhan, M.; Majewski, P. W.; Osuji, C. O. *Macromolecules* **2010**, *43* (7), 3286−3293.
(15) Singh, M.; Odusanya, O.; Wilmes, G. M.; Eitouni, H. B.; Gomez, E. D.; Patel, A. J.; Chen, V. L.; Park, M. J.; Fragouli, P.; Iatrou, H.; Hadjichristidis, N.; Cookson, D.; Balsara, N. P. *Macromolecules* **2007**, *40* (13), 4578–4585.
(16) Panday, A.; Mullin, S.; Gomez, E. D.; Wanakule, N.; Chen, V. L.; Hexemer, A.; Pople, J.; Balsara, N. P. *Macromolecules* **2009**, *42* (13), 4632–4637.
(17) Wanakule, N. S.; Panday, A.; Mullin, S. A.; Gann, E.; Hexemer, A.; Balsara, N. P. *Macromolecules* **2009**, *42* (15), 5642–5651.
(18) Young, W. S.; Epps, T. H. *Macromolecules* **2009**, *42* (7), 2672–2678.
(19) Gomez, E. D.; Panday, A.; Feng, E. H.; Chen, V.; Stone, G. M.; Minor, A. M.; Kisielowski, C.; Downing, K. H.; Borodin, O.; Smith, G. D.; Balsara, N. P. *Nano Lett.* **2009**, *9* (3), 1212–1216.
(20) Robitaille, C. D.; Fauteux, D. *J. Electrochem. Soc.* **1986**, *133* (2), 315–325.

(21) Lascaud, S.; Perrier, M.; Vallee, A.; Besner, S.; Prudhomme, J.; Armand, M. *Macromolecules* **1994**, *27* (25), 7469–7477.
(22) Vallée, A.; Besner, S.; Prud'Homme, J. *Electrochim. Acta* **1992**, *37* (9), 1579–1583.
(23) Papke, B. L.; Ratner, M. A.; Shriver, D. F. *J. Phys. Chem. Solids* **1981**, *42* (6), 493–500.
(24) Lee, Y. L.; Crist, B. *J. Appl. Phys.* **1986**, *60* (8), 2683–2689.
(25) Gray, F. M. *Polymer Electrolytes*; The Royal Society of Chemistry: London, 1997.
(26) Perrier, M.; Besner, S.; Paquette, C.; Vallee, A.; Lascaud, S.; Prudhomme, J. *Electrochim. Acta* **1995**, *40* (13−14), 2123–2129.
(27) Edman, L.; Doeff, M. M.; Ferry, A.; Kerr, J.; De Jonghe, L. C. *J. Phys. Chem. B* **2000**, *104* (15), 3476–3480.
(28) Andreev, Y. G.; Lightfoot, P.; Bruce, P. G. *Chem. Commun.* **1996**, No. 18, 2169–2170.
(29) Appetecchi, G. B.; Kim, G. T.; Montanina, M.; Carewska, M.; Marcilla, R.; Mecerreyes, D.; De Meatza, I. *J. Power Sources* **2010**, *195* (11), 3668–3675.
(30) Shin, J. H.; Henderson, W. A.; Passerini, S. *Electrochem. Solid State Lett.* **2005**, *8* (2), A125–A127.
(31) Shin, J. H.; Henderson, W. A.; Scaccia, S.; Prosini, P. P.; Passerini, S. *J. Power Sources* **2006**, *156* (2), 560–566.
(32) Shin, J.-H.; Henderson, W. A.; Passerini, S. *Electrochem. Commun.* **2003**, *5* (12), 1016–1020.
(33) Shin, J. H.; Henderson, W. A.; Passerini, S. *J. Electrochem. Soc.* **2005**, *152* (5), A978–A983.
(34) Kim, G. T.; Appetecchi, G. B.; Alessandrini, F.; Passerini, S. *J. Power Sources* **2007**, *171*, 861–869.
(35) MacFarlane, D. R.; Meakin, P.; Sun, J.; Amini, N.; Forsyth, M. *J. Phys. Chem. B* **1999**, *103* (20), 4164–4170.
(36) Simone, P. M.; Lodge, T. P. *ACS Appl. Mater. Interfaces* **2009**, *1* (12), 2812–2820.
(37) Zhu, C.; Cheng, H.; Yang, Y. *J. Electrochem. Soc.* **2008**, *155* (8), A569–A575.
(38) Cheng, H.; Zhu, C.; Huang, B.; Lu, M.; Yang, Y. *Electrochim. Acta* **2007**, *52* (19), 5789–5794.
(39) Leibler, L. *Macromolecules* **1980**, *13* (6), 1602–1617.
(40) Wang, J. Y.; Chen, W.; Russell, T. P. *Macromolecules* **2008**, *41* (13), 4904–4907.
(41) Wang, Z.-G. *J. Phys. Chem. B* **2008**, *112* (50), 16205–16213.
(42) Lodge, T. P.; Hanley, K. J.; Pudil, B.; Alahapperuma, V. *Macromolecules* **2003**, *36* (3), 816–822.
(43) Shibayama, M.; Hashimoto, T.; Hasegawa, H.; Kawai, H. *Macromolecules* **1983**, *16* (9), 1427–1433.
(44) Hashimoto, T.; Shibayama, M.; Kawai, H. *Macromolecules* **1983**, *16* (7), 1093–1101.
(45) Fredrickson, G. H.; Leibler, L. *Macromolecules* **1989**, *22* (3), 1238–1250.
(46) Hadjichristidis, N.; Iatrou, H.; Pispas, S.; Pitsikalis, M. *J. Polym. Sci., Part A: Polym. Chem.* **2000**, *38* (18), 3211–3234.
(47) Quirk, R. P.; Kim, J.; Kausch, C.; Chun, M. S. *Polym. Int.* **1996**, *39* (1), 3–10.
(48) Esswein, B.; Moller, M. *Angew. Chem., Int. Ed. Engl.* **1996**, *35* (6), 623–625.
(49) Noda, A.; Susan, M. A. B. H.; Kudo, K.; Mitsushima, S.; Hayamizu, K.; Watanabe, M. *J. Phys. Chem. B* **2003**, *107* (17), 4024–4033.
(50) Garetz, B. A.; Newstein, M. C.; Dai, H. J.; Jonnalagadda, S. V.; Balsara, N. P. *Macromolecules* **1993**, *26* (12), 3151–3155.
(51) Porter, C. H.; Boyd, R. H. *Macromolecules* **1971**, *4* (5), 589–&.
(52) Abraham, K. M.; Jiang, Z.; Carroll, B. *Chem. Mater.* **1997**, *9* (9), 1978–1988.
(53) Kumar, M.; Sekhon, S. S. *Eur. Polym. J.* **2002**, *38* (7), 1297–1304.
(54) Gray, F. M.; Vincent, C. A.; Kent, M. *J. Polym. Sci., Part B: Polym. Phys.* **1989**, *27* (10), 2011–2022.
(55) Yano, O.; Wada, Y. *J. Polym. Sci. Part A2: Polym. Phys.* **1971**, *9* (4), 669–&.
(56) Yu, S. Z.; Hing, P. *J. Appl. Polym. Sci.* **2000**, *78* (7), 1348–1353.
(57) Hanley, K. J.; Lodge, T. P.; Huang, C. I. *Macromolecules* **2000**, *33* (16), 5918–5931.
(58) Park, M. J.; Char, K.; Lodge, T. P.; Kim, J. K. *J. Phys. Chem. B* **2006**, *110* (31), 15295–15301.
(59) The appearance of a shoulder rather than a peak is probably due to the differences in instrument resolution at SSRL vs ALS. In general, the ALS has better resolution than SSRL. The samples with ImTFSI at $r = 0.05$ and higher were measured at SSRL. The rest of the samples were run at ALS.
(60) Lightfoot, P.; Mehta, M. A.; Bruce, P. G. *Science* **1993**, *262* (5135), 883–885.
(61) Londono, J. D.; Annis, B. K.; Habenschuss, A.; Borodin, O.; Smith, G. D.; Turner, J. Z.; Soper, A. K. *Macromolecules* **1997**, *30* (23), 7151–7157.
(62) Mao, G. M.; Saboungi, M. L.; Price, D. L.; Armand, M. B.; Howells, W. S. *Phys. Rev. Lett.* **2000**, *84* (24), 5536–5539.
(63) MacCallum, J. R.; Vincent, C. A. *Polymer Electrolyte Reviews*; Elsevier Applied Science Publishers: New York, 1987.
(64) Matsen, M. W.; Bates, F. S. *Macromolecules* **1996**, *29* (4), 1091–1098.
(65) Fredrickson, G. H.; Helfand, E. *J. Chem. Phys.* **1987**, *87* (1), 697–705.
(66) Bates, F. S.; Fredrickson, G. H. *Phys. Today* **1999**, *52* (2), 32–38.
(67) Matsen, M. W.; Schick, M. *Phys. Rev. Lett.* **1994**, *72* (16), 2660–2663.
(68) Cochran, E. W.; Garcia-Cervera, C. J.; Fredrickson, G. H. *Macromolecules* **2006**, *39* (7), 2449–2451.
(69) Lodge, T. P.; Pudil, B.; Hanley, K. J. *Macromolecules* **2002**, *35* (12), 4707–4717.
(70) Cochran, E. W.; Morse, D. C.; Bates, F. S. *Macromolecules* **2003**, *36* (3), 782–792.
(71) Zhu, L.; Cheng, S. Z. D.; Calhoun, B. H.; Ge, Q.; Quirk, R. P.; Thomas, E. L.; Hsiao, B. S.; Yeh, F.; Lotz, B. *Polymer* **2001**, *42* (13), 5829–5839.
(72) Jenkins, H. D. B.; Roobottom, H. K.; Passmore, J.; Glasser, L. *Inorg. Chem.* **1999**, *38* (16), 3609–3620.
(73) Gu, B.; Coates, J. D. *Perchlorate: environmental occurence, interactions and treatment*; Springer: New York, 2006.
(74) Krossing, I.; Slattery, J. M.; Daguenet, C.; Dyson, P. J.; Oleinikova, A.; Weingartner, H. *J. Am. Chem. Soc.* **2006**, *128* (41), 13427–13434.